CORE
Metadata, citation and similar papers at core.ac.uk
Provided by Missouri University of Science and Technology (Missouri S&T): Scholars' Mine

Missouri University of Science and Technology
Scholars' Mine

Electrical and Computer Engineering Faculty Research & Creative Works

Electrical and Computer Engineering

01 Jan 1991

A Laboratory Investigation of Electro-Optic Kerr Effect for Detection of Electric Transmission Line Faults

Badrul H. Chowdhury
Missouri University of Science and Technology, bchow@mst.edu

E. Grigsby

T. J. Englert

Follow this and additional works at: https://scholarsmine.mst.edu/ele_comeng_facwork

 Part of the Electrical and Computer Engineering Commons

Recommended Citation

B. H. Chowdhury et al., "A Laboratory Investigation of Electro-Optic Kerr Effect for Detection of Electric Transmission Line Faults," *IEEE Transactions on Power Delivery*, Institute of Electrical and Electronics Engineers (IEEE), Jan 1991.
The definitive version is available at https://doi.org/10.1109/61.85837

This Article - Journal is brought to you for free and open access by Scholars' Mine. It has been accepted for inclusion in Electrical and Computer Engineering Faculty Research & Creative Works by an authorized administrator of Scholars' Mine. This work is protected by U. S. Copyright Law. Unauthorized use including reproduction for redistribution requires the permission of the copyright holder. For more information, please contact scholarsmine@mst.edu.

A LABORATORY INVESTIGATION OF ELECTRO-OPTIC KERR EFFECT FOR DETECTION OF ELECTRIC TRANSMISSION LINE FAULTS

Thad J. Englert Member
Badrul H Chowdhury Member
Edward Grigsby Student Member

Department of Electrical Engineering
University of Wyoming
Laramie, WY 82071

ABSTRACT

A prototype Kerr cell has been constructed and tested for detecting and identifying faults by monitoring high voltages such as are found in electric power delivery systems. Simulated faults have been generated under laboratory conditions, monitored by the Kerr cell, and preliminary analysis done using analog-to-digital conversion of the detected waveforms with a single board microprocessor serially interfaced with a personal computer. The occurrence of faults is readily observed and results indicate that identification of fault types can be accomplished within less than one cycle of a standard sixty-cycle-per-second delivery system such as that found in the United States. With a dedicated analysis system such a technique may prove timely and economical in fault identification and location.

Keywords Kerr cell, voltage monitoring, synchronous generator, nitrobenzene.

1. INTRODUCTION

A primary objective of public utility electrical power systems is to maintain a high level of continuity of service. It is impossible to avoid accidental failure or misoperation due to human error and inadvertent connections or "flashover" between wires or from wires to ground along the delivery systems. Detection and analysis of the occurrence of such faults in these systems are critical to the timely maintenance of service.

Detection apparatus, prior to approximately the last decade, depended on inductive devices such as current transformers which consist of a simple coil surrounding the power line. These are susceptible to induced signals from other sources not necessarily associated with the power delivery system and are prone to give false indications of fault occurrences. With the advent of highly transparent optical waveguides (optical fibers) the possibility of fault sensing without electromagnetic interference became more feasible. A variety of methods using optical techniques and the linear Pockels effect have since been reported which exhibit relatively good success in fault detection [1,2,3,4]. The analysis schemes of many of the techniques seem unnecessarily complicated however. The linear electro-optic effect has also been used in field distribution measurements in transformer applications [5].

In this paper we describe a prototype cell, which uses the non-linear Kerr effect in nitrobenzene, for detection of fault occurrences, and show the resulting waveforms and associated frequency spectra of the optical intensity modulated by the monitored electric potentials including steady-state and laboratory-generated voltage faults. Non-linear or Kerr effect electro-optic techniques have been used for a variety of applications in sensing electric fields but have been primarily aimed at field mapping. These field mapping studies make use of the repetitive behavior, sometimes called fringing, of the phase retardation of lightwaves whose electric fields are polarized in the direction of the external electric field imposed on the electro-optic material. "Fringing" in this context is not to be confused with fringing due to lightwave interference or diffraction patterns. Rather, the fringing alluded to is caused by the external electric field passing through multiples of the field value which yields the first maximum optical response [6-13]. The experiments described here are designed to monitor simulated line voltages at or below electric field magnitudes yielding the first maximum optical response.

91 WM 017-4 PWRD A paper recommended and approved by the IEEE Power System Instrumentation & Measurements Committee of the IEEE Power Engineering Society for presentation at the IEEE/PES 1991 Winter Meeting, New York, New York, February 3, 1991. Manuscript submitted February 1, 1990; made available for printing December 11, 1990.

2. KERR CELL DETECTION

2.1 Principle of Operation

The Kerr effect differs from the Pockels effect in that the birefringence in the Kerr material depends on the square of the electric field in the material rather than a linear dependence found in the Pockels effect. Birefringence induced by the presence of an electric potential applied to electrodes separated by the Kerr material causes the orthogonal components of polarization of the electric field of light passing through the material to travel at different speeds. As such, when the light passing through the cell reaches the exit the two components of polarization are out of phase causing varying degrees of elliptic polarization, depending on the applied potential. A polarizer placed at the optical output end of the cell then transmits light whose intensity depends upon the alignment of the axes of the elliptically polarized light incident on the polarizer.

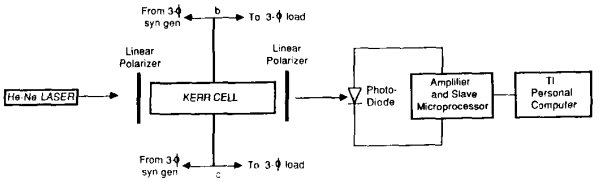

Figure 1. Block diagram of the experimental system

Voltages applied across the Kerr cell are the line-to-line voltages of a balanced three-phase system. In Fig. 1 the voltage across lines b and c are shown applied to the cell which is the configuration throughout the series of tests reported herein. Functional descriptions of the data acquisition system at the output side of the Kerr cell are given in later sections of this paper. The difference in the indices of refraction for the two components of lightwave polarization for the Kerr effect, is given by

$$n_p - n_s = K\lambda_o E^2 \tag{1}$$

where n_p is the index of refraction of light whose electric field is polarized parallel to the direction of the externally applied electric field, n_s is the index for the polarization component perpendicular to the field, λ_o is the vacuum wavelength of the light passing through the cell, E is the electric field applied to the Kerr material, and K is the Kerr coefficient. It should be noted here that the electric field, E, includes that of the light whose electric field is assumed to be small compared to the externally applied field. With relatively low intensity light, this field may be taken to be only that due to the high voltage field being measured. Light linearly polarized at an angle of 45° to the direction of the electric field applied to the cell gives equal polarization components parallel to and perpendicular to the externally applied field. This light is launched into the Kerr cell and becomes elliptically polarized, due to relative phase differences suffered by the two propagating components of polarization, with the degree of ellipticity dependent upon the strength of the field. Figure 1 depicts a sketch of the Kerr cell along with polarizing elements. If the electric field of the incident polarized lightwave is given by

$$\vec{E} = \vec{E_o}\cos(kz - wt) \tag{2}$$

with the direction of the field at 45° to the input polarizer axis, then the components of the field as the light propagates through the medium is found to be

$$E_x = \frac{E_o}{\sqrt{2}}\cos\left(\frac{2\pi}{\lambda_o} n_p z - \omega t\right) \tag{3}$$

and

$$E_y = \frac{E_o}{\sqrt{2}}\cos\left(\frac{2\pi}{\lambda_o} n_s z - \omega t\right) \tag{4}$$

0885-8977/91/0700-0979$01.00©1991 IEEE

As the lightwave propagates through the Kerr medium a phase difference results between the orthogonal components of polarization resulting in an elliptically polarized state. If, after traveling through a length L of the Kerr medium the light is passed through a second polarizer which is oriented orthogonally to the input polarizer, the output optical intensity is found to be

$$I = I_o \sin^2 [\pi L K V^2/d^2] \quad (5)$$

where I_o is the maximum transmitted light intensity, V is the electric potential difference between the Kerr cell electrodes, L is the effective length of the light path through the cell, and d is the effective dimension of the cell in the direction of the externally applied field. Equation 5 is often written as

$$I = I_o \sin^2 \left[\frac{\pi}{2}\left(\frac{V}{V_m}\right)^2\right] \quad (6)$$

where V_m is given by [10]

$$V_m = d(2LK)^{-1/2} \quad (7)$$

Taking the source of the externally applied potential to be a line-to-line voltage, in these experiments, of the electrical power delivery system measured, we may write this potential as

$$V = V_o \sin(\omega t) \quad (8)$$

where V_o is the maximum voltage of the power line. The potential of Eq. 8 is allowed to appear across the Kerr cell giving rise to a time varying field within the cell, thus yielding a variation in output light intensity exiting the cell according to Eq. 6. The experimental work described in this paper restricts the applied potential to $V \leq V_m$ and the Kerr cell is designed accordingly.

2.2 Design of the Prototype Kerr Cell

The coefficients for electro-optic modulation of light, such as those found in the Kerr effect are typically small. For nitrobenzene, the material chosen for this work since the Kerr coefficient is relatively large, K is approximately $3.16 \times 10^{-12} m/V^2$. Small applied potentials therefore make the cell dimensions prohibitively small. A power laboratory three phase, 2-pole synchronous generator rated at 120 volts and 5 kVA is used to drive a transformer to yield a maximum potential of 3,500 volts at 60 Hz. The Kerr cell is therefore designed for a voltage of 3,500 volts. A rectangular cross section glass tubing having an inner dimension, d, of 0.6 mm, cut to a length of 43.2 cm, is filled with nitrobenzene and copper electrodes placed above and below the tube. The thickness of the glass tubing must be accounted for in calculation of the electric field in the nitrobenzene. A straight-forward calculation using electric field continuity conditions across dielectric boundaries gives the electric field,E which appears in Eq. 1, within the nitrobenzene as

$$E = \frac{V}{d + \frac{2\varepsilon d_g}{\varepsilon_g}} \quad (9)$$

where V is the voltage appearing across the Kerr cell, d is the thickness of the nitrobenzene, ε is the dielectric constant of the nitrobenzene, d_g is the thickness of the glass tubing wall, and ε_g is the dielectric constant of the glass. Field fringing has been ignored. The 60 Hz, 3,500 volt peak output of the transformer is then applied to the cell electrodes. A low power helium-neon laser is used as the light source, the unpolarized laser beam being passed through a polarizer at the input of the cell with the polarization at 45° to the electric field created by the transformer voltage.

A second polarizer, orthogonally oriented with respect to the input polarizer, then gives zero output light intensity when the applied voltage passes through zero. Maximum light intensity output occurs when the applied potential passes through its maximum of 3,500 volts, the design of the Kerr cell being such that V_m = 3,500 volts thereby avoiding fringing orders greater than 1.

Figure 2 shows the Kerr cell and Figure 3 shows a typical output of measured light intensity for the system in the steady state (no faults). It should be noted that the output optical intensity represents a rectified version of the voltage applied to the Kerr cell, however the rectified wave is not that found in the usual sense because of the square of the sine functions found in the intensity described by Eqs. 5 and 6. Some optical noise is evident in the curve of Figure 3 which was found to be due to variation in the light intensity from the laser. This variation is caused by ripple in the rectified power supply driving the laser and has a frequency of 120 Hz. Later versions of this system will use a more constant intensity source of light such as a laser diode or light-emitting diode.

2.3 Detection and Conversion of the Optical Output

The data acquisition system consists of a master-slave type interface of a single board, 8086 microprocessor (slave) and a Texas Instrument (TI) personal computer (master). Appropriate code control routines are routed through a serial interface from the TI to the microprocessor allowing A/D conversion and data storage.

A PIN photo-diode is used to detect the optical signal with the amplified output fed into a sample and hold for the A/D conversion. The conversion rate is set at 1800 samples per second by the master and a total of 4096 samples (2.27 seconds) accumulated, corresponding to 30 samples for each cycle of 60 Hz signal, and stored in RAM of the slave board. According to principles of digital signal processing, a signal is uniquely represented if (Nyquist criteria) [14]

$$f_s \geq 2f \quad (10)$$

where f_s is the sampling frequency and f is the frequency component in the sampled signal. At 1800 samples per second corresponding to 30 samples per cycle, zero mean square error is anticipated for signal frequency components as large as 900 Hz [14]. Frequencies due to fault conditions introduced into the signal may then be reliably sampled up to 900 Hz. The reader is reminded that the steady-state optical signal being monitored has a frequency of 120 Hz, as discussed earlier. Any frequency components greater than 900 Hz will lead to "aliasing" in the signal processing. To avoid aliasing, a simple low-pass R-C filter with a 3-dB point at 795 Hz and a 20-dB per decade slope after the corner frequency, is used. This anti-aliasing filter effectively reduces frequency component contributions above 900 Hz to a negligible level. The likelihood of fault induced frequencies above this frequency is assumed to be remote.

Start of conversion is controlled by the master and monitored with a LED to indicate to the operator that conversion is taking place. After conclusion of the conversion, the data stored in RAM of the slave is transmitted to the master via the serial port and stored on hard disk by the master. A block diagram of the electronics and computer controlled data acquisition system is shown in Fig. 4.

2.4 Signal Conditioning and Processing

Voltage data, transduced by the Kerr cell, for the steady state was found to vary somewhat in amplitude due to light intensity variation from the laser source as noted earlier. To alleviate this minor effect, the data are normalized to yield maxima and minima of +1 and -1 respectively. Normalization was accomplished by determining the maximum and minimum amplitudes within a given data set, dividing every data point by the maximum after subtraction of the minimum from every data point. The final step in normalization subtracted the mean value determined from the steady-state signal, which preceeded the fault, in the data set from all other points of the set. This normalization then allows easy comparison of relative amplitudes and spectral energy of various frequency components, including dc components, during successive fault tests.

Data sequences produced by the normalization routine are then analyzed for spectral energy density by using the Discrete Fourier technique (DFT). A rectangular window function is used, the original data sequence being blocked into 32-point sections, each section overlapping by 16 data points. This window width represents approximately one full cycle of the original 60 Hz high-voltage signal while moving the window 16 data points for successive analyses will represent a DFT during each half cycle of the 60 Hz signal. Each block, or window, is then padded with 96 zeroes to increase the output resolution of the spectral estimation routine which produces estimations with a fundamental of 14 Hz and 64 discrete frequency components. This padding has been added to reduce "leakage" which typically occurs in DFT calculations using rectangular windows [15]. Remnants of leakage effects are evident in the data presented below, however these effects are not so large as to mask the data of interest. In principle it would be possible to include more data points but computation time increases accordingly for each DFT, which defeats the ultimate aim of real-time analysis. The integral power of two data points within the analysis window has been chosen for computational convenience in the DFT algorithm used.

3. TEST RESULTS

Several tests were conducted on a power laboratory, three-phase synchronous generator to investigate the behavior of the optical fault detector under different fault conditions. The generator was configured as a wye-connected, 120V line-to-line generation system transformed to 2475V (3500 peak) as described earlier, with its neutral solidly grounded. The experimental set-up for conducting faults on a loaded generator is shown in Fig. 1, in Section 2 of this paper. The simulation of power line faults is accomplished by causing line-to-ground or line-to-line contacts in electrical power delivered by the generator.

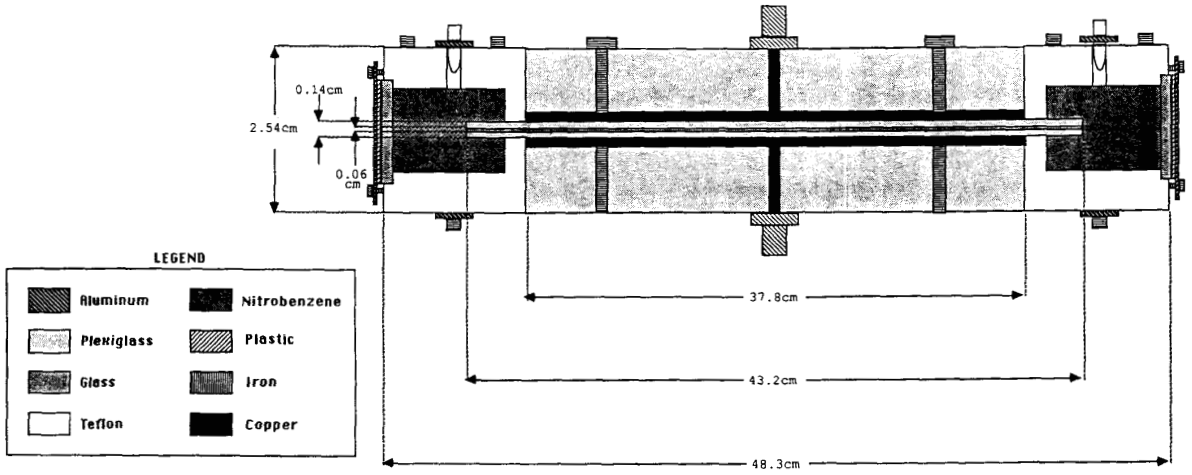

Figure 2. A cross-sectional view of the Kerr cell

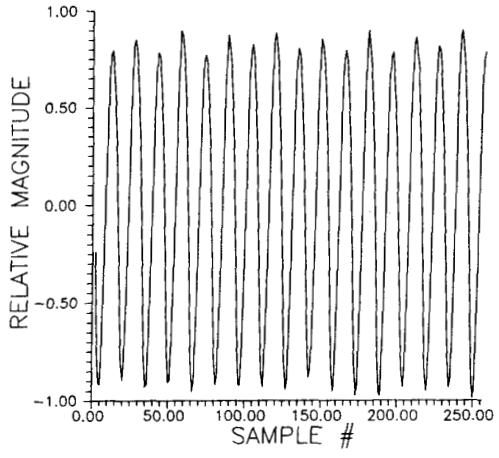

Figure 3. Recorded output of the Kerr cell during steady-state

The following is a list of the fault studies conducted:

a) Single line to ground fault on the loaded generator.
b) Line-to-line fault on the loaded generator.
c) Double line-to-ground fault on the loaded generator.
d) Three phase fault on the loaded generator.

The objectives of the tests are the identification of certain distinctive characteristics from the output of the Kerr cell for all the different fault conditions. As noted earlier, the Kerr cell is connected across the b and c phases.

A graph of the light intensity output during the time of an introduced line-to-ground fault, and until recovery after removal of the fault, is shown in Figure 5. Three successive DFT analysis windows, described earlier, are outlined within the figure. Window 1 is the pre-fault zone, window 2 contains the point of application of the fault and window 3 is the post-fault zone. Each window is 2 cycles (of 120 Hz) wide and the windows overlap a half cycle. Shifting the windows across the acquired samples allows investigation of the evolution of the spectral content. Due to the large temporal variations in the samples at the point of application of the fault and beyond, the spectral contents of the three windows vis-a-vis pre-fault, during fault, and post-fault windows, will show different spectral characteristics. In the following analysis, we attempt to demonstrate the susceptibility of fault identification to the spectral information contained within such windows.

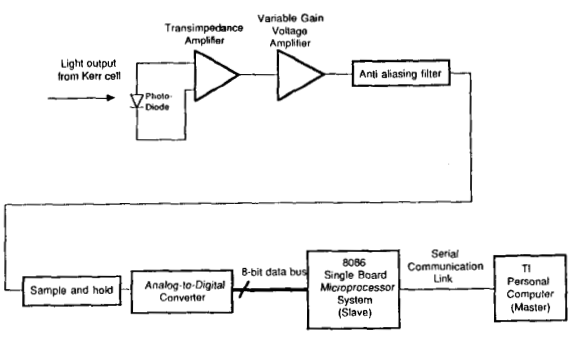

Figure 4. The data acquisition system

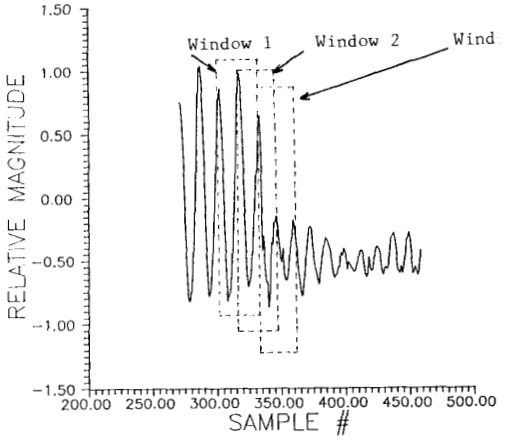

Figure 5. Recorded output of the Kerr cell during line-to-ground fault

A graph such as Fig. 5 is obtained for each fault type. A 2-cycle window is then traversed across the entire graph. Using the signal conditioning procedure as described in Section 2.4, the discrete points inside each window are subjected to a Discrete Fourier Transform (DFT). This information is plotted on a three-dimensional diagram as shown in Figure 6a for a single line-to-ground fault on the system. In this figure, each of the smallest marks on the "Time Window" axis corresponds to 8.33 msec. Figure 6a clearly shows the identification of a fault in the power system after 0.5 secs from the origin of the plot.

Figure 6b, c and d show the frequency spectrum as a result of the application of DFT to each of the three windows 1, 2 and 3 respectively for the same fault as portrayed in Fig. 6a. To repeat, these windows correspond to pre-fault, during-fault and post-fault conditions respectively. Figures 7 through 9 show the same set of information for other types of faults. Marked differences in frequency components and/or amplitudes can be observed in each of the figures. The salient points are tabulated in Table 1. Care was taken so that each test was conducted repeatedly under similar conditions, which included performance of the laser gun, frequency of the generator, load on the generator, voltage generated by the generator, the faulting device, etc. Due to degradation of the performance of the laser gun, one of the tests, namely fault between lines a and b, could be conducted only once and hence no conclusion could be drawn on that particular fault.

From the table, it is evident that the type of fault, meaning whether it is a phase fault or a ground fault can be differentiated by observing certain characteristics. Of course, the characteristics should be investigated with regard to the location of the Kerr cell across specific lines. It appears that, since the cell was connected across lines b and c, any fault involving these two phases will have a relatively large impact on the 120-Hz component. In other words, this component will shrink considerably in both the fault and post-fault windows. This particular effect is sharply noticeable when the two phases are faulted alone either to each other or to ground. Also from the table, the double line-to-ground faults consistently produce a second frequency component higher than the 120-Hz and the latter is reduced to almost nil in the post-fault window. On the other hand, the three-phase fault produces a rather clean 120-Hz frequency component in the fault and post-fault windows. Presence of a dc component in any of the spectra is due to the fact that the datum of the sampled data is shifted either during or after fault. It should be pointed out that in all fault cases, voltage collapse is maintained consistently in the post-fault window, which means that a significant amount of time is available to allow distinction between a fault and a transient on the system.

4. CONCLUSIONS AND DISCUSSION

A prototype Kerr cell has been constructed and tested for monitoring high voltages and identifying faults in power systems. Simulated faults were generated under laboratory conditions using a power laboratory synchronous generator and monitored by the Kerr cell. Results can be extended to any larger systems such as are found in typical electric power delivery systems in the U.S.

The occurrence of faults is readily observed by inspection of light intensity outputs during the time of an introduced fault, however it it is evident from the spectral analyses that fault types are identifiable which may not be immediately evident in the time domain data. Discrete Fourier techniques were used to analyze the spectral energy density in the data sequence produced by the Kerr cell before the fault , during the fault and after the fault. Investigation of the results produced by various types of faults in the system reveals the fact that the Kerr cell identifies significant differences between the phase faults and the ground faults. The position of the Kerr cell between two particular phases, is very important in the analysis. During the investigations, the Kerr cell was connected between phases b and c. As a result, the b and c lines-to-ground fault and the b-to-c line fault appear to have similar frequency components. This might be expected because in both cases the Kerr cell apparently looks at a collapsed voltage across its terminals. On the other hand, the line a-to-ground and line b-to-ground faults are quite different, each having distinctive features. The ground faults, in general produce large dc components during and after the faults. In any case, the spectral components of various fault types exhibit marked differences. The test spectra show general consistency when experiments are repeated under identical laboratory conditions.

Table 1. Simulation of Faults

Fault	Remarks
Line a-to-ground	The 120-Hz component reduces to 89% of the prefault condition during fault and to 64% in the post-fault window. No significant dc component is present in the three windows. Presence of two humps at 600-Hz and 700-Hz. It is believed that these two frequency components are due to the non-linear excitation of the transformer across the other two phases. The two high frequency components are absent in the other two line-to-ground faults.
Line b-to-ground	The 120-Hz component reduces to 83% of the prefault condition during fault and to 43% in the post-fault window. Presence of large dc component in post fault window signifying that there is a shift of datum after the voltage starts to recover.
Line c-to-ground	The 120-Hz component reduces to 22% of the prefault condition during fault and maintains this magnitude in the post-fault window. Presence of large dc component in both fault and post fault windows signifying that there is a shift of datum during and after the voltage recovery.
Line a-to-c	The 120-Hz component reduces to 65% of the prefault condition during fault and to 50% in the post-fault window. This component is predominant in all windows. No significant dc component is present in the three windows.
Line b-to-c	The 120-Hz component reduces to 35% of the prefault condition during fault and to an undetectable level in the post-fault. Presence of a large dc component in the post-fault window is due to the same reason as noted earlier. The 120-Hz component is not predominant. A frequency component higher than 120-Hz is present in window 2.
Lines a & b-to-ground	The 120-Hz component reduces to 47% of the prefault condition during fault and to 8% in the post-fault window. Presence of a large dc component in window 3. The 120-Hz component is not predominant. A frequency component higher than 120-Hz is present in window 2.
Lines b & c-to-ground	The 120-Hz component reduces to 53% of the prefault condition during fault and to 22% in the post-fault window. Presence of a large dc component in window 3. The 120-Hz component is not predominant. A frequency component higher than 120-Hz is present in window 2. Frequency components are nearly identical to "line b-to-c" fault case. However amplitudes may be significantly different.
Lines a & c-to-ground	The 120-Hz component reduces to 38% of the prefault condition during fault and to 5% in the post-fault window. Presence of a large dc component in window 3. The 120-Hz component is not predominant. A frequency component higher than 120-Hz is present in window 2.
Three-phase fault	The 120-Hz component reduces to 63% of the prefault condition during fault and to 16% in the post-fault window. Presence of a large dc component in window 3. The 120-Hz component is predominant in all windows.

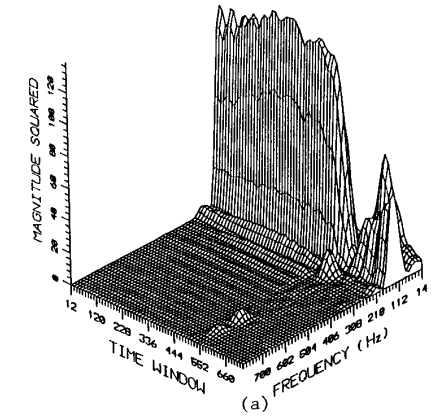

(a)

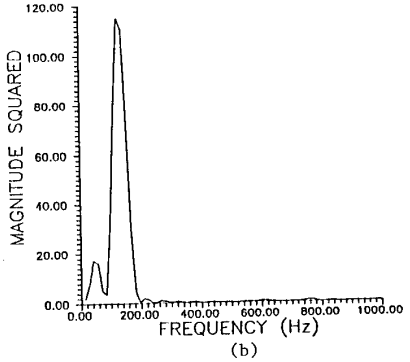

(b)

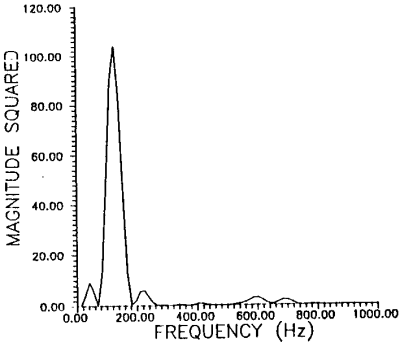

(c)

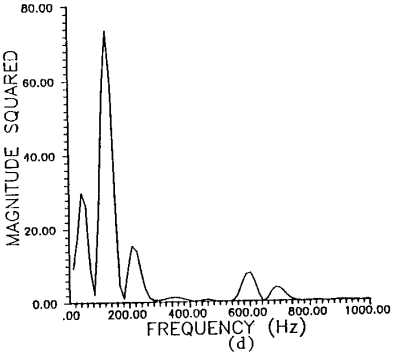

(d)

Figure 6. Line a-to-ground fault

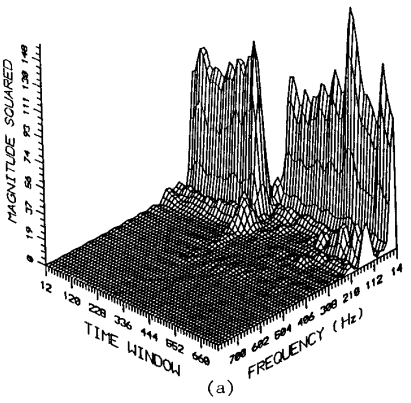

(a)

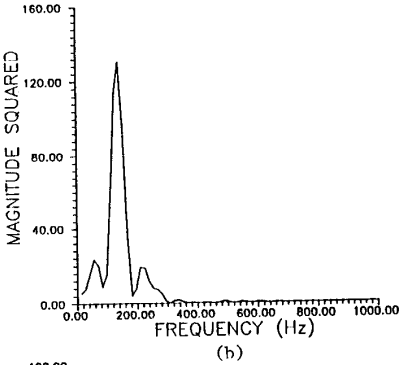

(b)

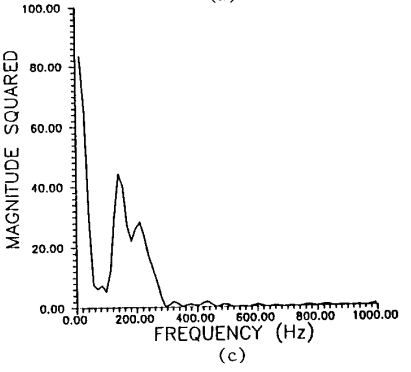

(c)

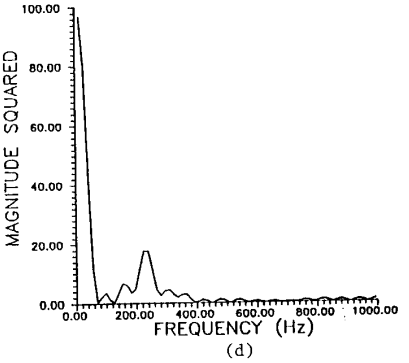

(d)

Figure 7. Double line b-to-c fault

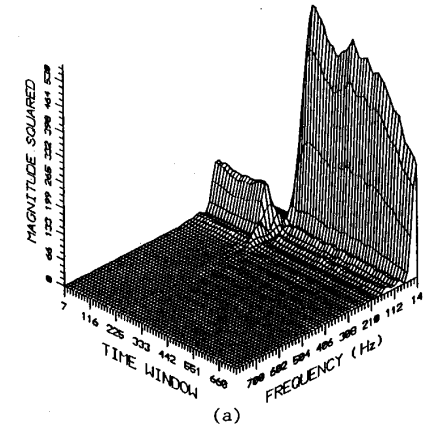

(a)

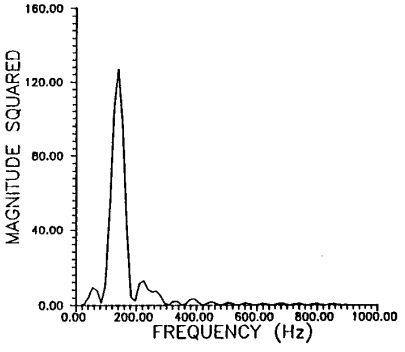

(b)

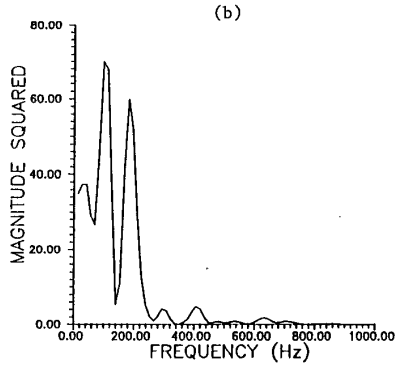

(c)

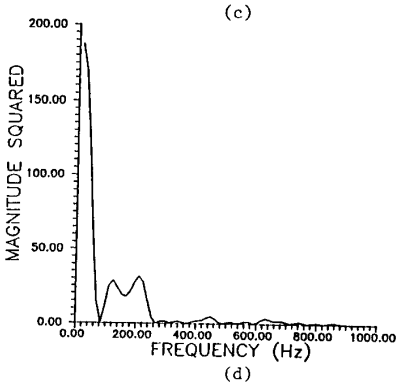

(d)

Figure 8. Double line b-and-c-to-ground fault

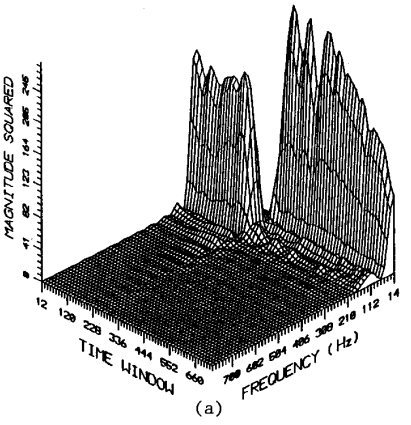

(a)

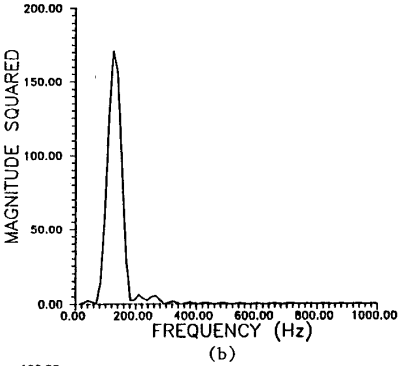

(b)

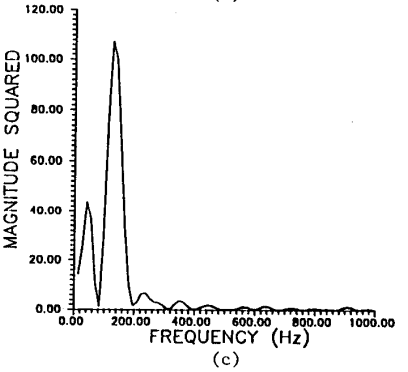

(c)

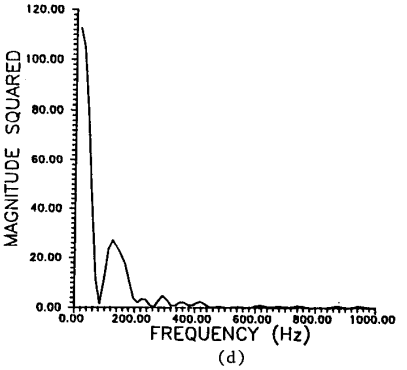

(d)

Figure 9. Three-phase fault

The use of nitrobenzene in these experiments was dictated primarily by availability, economics, and the relatively large Kerr coefficient. Off-the-shelf research quality nitrobenzene having a purity of 99% or greater and available from most chemical supply companies, was used . No deterioration in performance was noted during the course of this work which lasted for a period of approximately six months. This may in part be attributable to the use of borosilicate glass and teflon, although no special precautions other than ordinary laboratory cleanliness were taken. If the nitrobenzene is not exposed to contaminants, such as air and water, and dielectric breakdown is avoided, one would anticipate a relatively long lifetime expectancy. A year old cell used in shutter applications was found to have an electrical conductivity of 2.5×10^{-10} mhos/cm^3 compared to 7×10^{-11} mhos/cm^3 for pure nitrobenzene [16]. Some detrimental timing effects have been noted in previous work when sodium silicate (water glass) was used for confinement of nitrobenzene used in fast ($\sim 4 \times 10^{-9}$ sec) electro-optical shutter applications [16]. The melting point (5.7°C) [17] and thermal dependence of the refractive index [18] of nitrobenzene places considerable restriction on its use in Kerr cells in field applications. Under laboratory conditions wherein proof of principle is being demonstrated, such as reported here, temperature effects do not present any undue complications, however for field use of the techniques presented, more appropriate materials may be available with some sacrifice of Kerr coefficient.

Fault location in a power delivery line will determine the impedance between the power source and the fault which would be expected to be reflected in the relative intensity of the frequency components introduced by the fault. Conceivably the spectral information available in such a monitoring system as described here will prove useful in fault identification and location. With the fast digital chip technology available, real-time monitoring using these techniques should be possible. No attempts have been made to determine the impedances corresponding to the various fault conditions described herein.

Future experiments and computer simulations are planned which will incorporate simultaneous voltage and current measurements using electro-optic and magneto-optic effects. It is expected that more specific identification of faults will be possible as well as fault location, based on spectral information gleaned from fault data.

Acknowledgements

This research work was made possible by a grant from the University of Wyoming research office.

5. REFERENCES

1. G.A. Massey, J.C. Johnson, D.C. Erickson "Laser Sensing of Electric and Magnetic Fields for Power Transmission Applications" *SPIE*, Vol. 88, Polarized Light, 91-95, 1976.

2 M. Kanoi, G. Takahashi, T. Sato, M. Higaki, E. Mori and K. Okumura, "Optical Voltage and Current Measuring System For Electric Power Systems", *IEEE Transactions on Power Delivery*, Vol. PWRD-1, 91-97, Jan 1986.

3. T. Mitsui, K. Hosoe, H. Usami, S. Miyamoto, "Development of Fiber-Optic Voltage sensors and Magnetic Field Sensors", *IEEE Transactions on Power Delivery*, Vol. PWRD-2, 87-93, Jan 1987.

4. G.A. Massey, D.C. Erickson, and R.A. Kadlec, "Electromagnetic Field Components: Their Measurement Using Linear Electrooptic and Magnetooptic Effects", *Applied Optics*, Vol. 14, 2712-2719, Nov 1975.

5. S.J. Huang and D.C. Erickson, "The Potential use of Optical Sensors for the Measurement of Electric Field Distribution", *IEEE Transactions on Power Delivery*, Vol. 4, 1579-1585, July 1989.

6. J.E. Thompson, M. Kristiansen, M.O. Hagler, "Optical Measurement of High Electric and Magnetic Fields", *IEEE Transactions on Instrumentation and Measurement*, Vol. 25, No. 1, 1-7, Mar 1976.

7. G.R. Allen, H.P. Davis, B.T. Neyer, D.J. Muron, J. Chang, "Electro-optical Kerr Effect Voltage Measurements on Multi-megavolt Pulsed Power Accelarators", *SPIE*, Vol. 566, Fiber Optics and Laser Sensors III, 223-226, 1985.

8. M. Zahn, T. Takada, "High Voltage Electric Field and Space-charge Distributions in Highly Purified Water", *Journal of Applied Physics*, Vol. 54, No. 9, 4762-4775, Sept 1983.

9. R. E. Hebner, Jr., E.C. Cassidy, "Measurement of 60 Hz Voltages Using the Kerr Effect", *Review of Scientific Instruments*, Vol. 43, No. 12, 1839-1841, Dec 1972.

10. R.E. Hebner, Jr., R.A. Malewski, and E.C. Cassidy, "Optical Methods of Electrical Measurement at High Voltage Levels", *Proceedings of the IEEE*, Vol. 65, 1524-1548, Nov 1977.

11. E.F. Kelley and R.E. Hebner, "Electro-Optic Measurement of the Electric Field Distribution in Transformer Oil", *IEEE Transactions on Power Apparatus and Systems*, Vol. PAS-102, 2092-2097, July 1983.

12. E.C. Cassidy, W.E. Anderson, and S.R. Booker, "Recent Refinements and Developments in Kerr System Electrical Measurement Techniques", *IEEE Transactions on Instrumentation and Measurement*, Vol. IM-21, 504-510, Nov 1972.

13. E.C. Cassidy and H.N. Cones, "A Kerr Electro-Optical Technique for Observation and Analysis of High-Intensity Electric Fields", *J. of Research of the National Bureau of Standards-C. Engineering and Instrumentation*, Vol. 73C, 5-13, Jan-June, 1969.

14. J.G. Proakis, *Digital Communications*, Second Ed., McGraw-Hill Book Company, New York, 1989.

15. R.E. Ziemer, W.H. Tranter, and D.R. Fannin, *Signals and Systems: Continuous and Discrete*, Second Ed., Macmillan Publishing Company, New York, 1989.

16. F.G. Dunnington, "The Electrooptical Shutter-Its Theory and Technique", *Physical Review*, Vol. 38, 1506-1534, Oct 1931.

17. R.C. Weast, editor, *Handbook of Chemistry and Physics, 53rd Edition*, The Chemical Rubber Co., Cleveland, OH.

18. M. Mouton, "Electric and Magnetic Birefringence", in *International Critical Tables of Numerical Data; Physics, Chemistry and Technology*, Vol. 7, 109-113, 1930.

Thad L. Englert was born in Garden City, Kansas on November 14, 1934. He received his B.S. degree in Physics from the University of Northern Colorado in 1962, M.S. in Physics from Iowa State University in 1965, and Ph.D. in Physics from the University of Wyoming in 1983. Between the master's and doctoral degrees, he worked for four years at the Iowa State Synchrotron facility and for six years teaching at Colorado Mountain College at Glenwood Springs, CO.

He is currently an Assistant Professor of Electrical Engineering at the University of Wyoming. His research interests include electro-optics, non-linear optics and optical waveguides.

Dr. Englert is a member of IEEE, SPIE, ASEE and AAPT.

Badrul H. Chowdhury(M-87) received his Bachelor of Science degree in Electrical Engineering from the Bangladesh University of Engineering and Technology in 1981. He Obtained his M.S. in 1983 and his Ph.D. in 1987, both in Electrical Engineering from Virginia Polytechnic Institute and State University. He joined the Electrical Engineering department of the University of Wyoming in 1987 where he is currently an Assistant Professor.

Dr. Chowdhury has been actively involved in research in the area of Power Engineering for a number of years. His major areas of research interests are in power system planning, and operation, expert systems and alternate energy systems. He is the author of several technical papers in these areas.

Dr. Chowdhury is a member of IEEE and ASEE.

Ed Grigsby(S '86) was born in New Castle, Wyoming on August 1, 1964. He received his B.S. and M.S. degree in Electrical Engineering in 1988 and 1990 respectively, from the University of Wyoming. He is currently working at the Edwards Air Force Base in California. His present research interest in in electro-optics.

Mr. Grigsby is a member of IEEE and a member of LEOS.